The Predominance of Hydrogen Evolution on Transition Metal Sulfides and Phosphides under CO2 Reduction Conditions: An Experimental and Theoretical Study

Landers, Alan T.; Fields, Meredith; Torelli, Daniel A.; Xiao, Jianping; Hellstern, Thomas R.; Francis, Sonja A.; Tsai, Charlie; Kibsgaard, Jakob; Lewis, Nathan S.; Chan, Karen

Published in:
ACS Energy Letters

Link to article, DOI:
10.1021/acsenergylett.8b00237

Publication date:
2018

Document Version
Peer reviewed version

The Predominance of Hydrogen Evolution on Transition Metal Sulfides and Phosphides Under CO_2 Reduction Conditions: An Experimental and Theoretical Study

Alan T. Landers,[a, b, 1] Meredith Fields,[b, c, 1] Daniel A. Torelli,[d, 1] Jianping Xiao,[b, c] Thomas R. Hellstern,[b, c] Sonja A. Francis,[d] Charlie Tsai,[b, c] Jakob Kibsgaard,[b, c, e] Nathan S. Lewis,[d, 2] Karen Chan,[b, c, 2] Christopher Hahn,[b, c, 2] Thomas F. Jaramillo[b, c, 2]

a. Department of Chemistry, Stanford University, Stanford, CA 94305
b. SUNCAT Center for Interface Science and Catalysis, SLAC National Accelerator Laboratory, Menlo Park, CA 94025
c. Department of Chemical Engineering, Stanford University, Stanford, CA 94305
d. Division of Chemistry and Chemical Engineering, California Institute of Technology, Pasadena, CA 91125
e. Department of Physics, Technical University of Denmark, DK-2800 Kongens Lyngby, Denmark

1. A.T.L, M.F., and D.A.T. contributed equally to this work.
2. To whom correspondence should be addressed: N.S.L. nslewis@caltech.edu, K.C. chank@stanford.edu, C.H. chahn@slac.stanford.edu, T.F.J. jaramillo@stanford.edu

Abstract

A combination of experiment and theory has been used to understand the relationship between the hydrogen evolution reaction (HER) and CO_2 reduction (CO_2R) on transition metal phosphide and transition metal sulfide catalysts. Although multifunctional active sites in these materials could potentially improve their CO_2R activity relative to pure transition metal electrocatalysts, under aqueous testing conditions, these materials showed a high selectivity for the HER relative to CO_2R. Computational results supported these findings, indicating that a limitation of the metal phosphide catalysts is that the HER is favored thermodynamically over CO_2R. On Ni-MoS_2, a limitation is the kinetic barrier for the proton-electron transfer to *CO. These theoretical and experimental results demonstrate that selective CO_2R requires electrocatalysts that possess both favorable thermodynamic pathways and surmountable kinetic barriers.

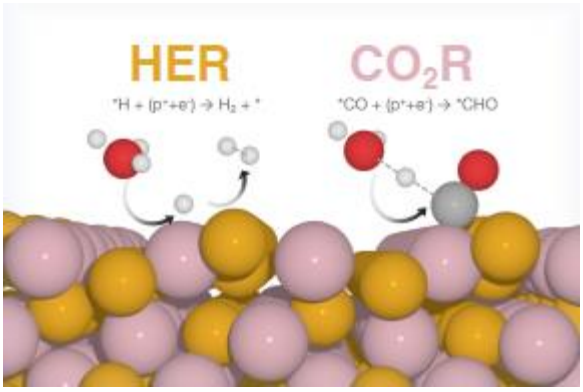

Electrochemical carbon dioxide reduction (CO_2R) has drawn interest for converting CO_2 into energy dense fuels such as ethanol, thereby providing an option for sustainable chemically based energy storage and building blocks for the chemical industry.[1-6] In aqueous solutions, CO_2R must compete with the kinetically more facile hydrogen evolution reaction (HER). The relative Faradaic efficiencies for the two reactions reflect the low ratio between the concentration of dissolved CO_2 in water and the concentration of protons and/or water that are the reactants for CO_2R and the HER, respectively, as well as the lower kinetic barriers for the two-electron reduction of water to H_2 relative to the multi-electron reduction of CO_2 to alcohols, olefins, or hydrocarbons. These factors generally lead to low selectivity for CO_2R. Understanding the competition between these reactions is critical to the development of more effective catalysts for CO_2R.

To facilitate large-scale adoption, CO_2R catalysts need to be developed that can selectively synthesize high value products at low overpotentials.[2-3] Polycrystalline copper electrocatalysts can reduce CO_2 to desirable products such as ethanol but also produce at least fifteen other products.[7] Competition between CO_2R and the HER further reduces the overall Faradaic efficiency toward any specific CO_2R product.[4,8] In addition to selectivity challenges, at present CO_2R electrocatalysts require substantial overpotentials to directly reduce CO_2 beyond CO or formate, leading to poor energy efficiency.[1,4,7] On transition metal (TM) electrocatalysts, thermodynamic calculations suggest that the high overpotential needed to drive CO_2 reduction beyond CO results in part from the linear scaling between the CO and CHO binding energies.[9] Subsequent *ab initio* calculations of the energetics of CO reduction to CH_4 show that the linear scaling between the CO binding energy and the transition state energy for proton-electron transfer to CO creates additional kinetic limitations on the activity of TM electrocatalysts for CO or CO_2 reduction.[10-11] These studies

indicate that favorable thermodynamics for the binding of reaction intermediates are necessary but perhaps insufficient criteria for achieving high activity and selectivity for CO_2R. Thus, obtaining a deeper understanding of the competition between CO_2R and the HER will require analyzing both the thermodynamics and the kinetics of reaction pathways.

The multifunctional active sites in TM phosphides or TM sulfides could serve as possible motifs for circumventing the aforementioned scaling relations.[9,12] In the context of hydrotreating reactions, the behavior of phosphide surfaces can be described by acidic functionality that is associated with phosphorus sites, in addition to metallic catalytic functionality associated with the metal sites.[13] This bifunctional characteristic, along with the high degree of polarity between the cationic and anionic constituents, could, through secondary bonding interactions, selectively stabilize the H-CO transition state relative to adsorbed CO. Interaction with S or P non-metal sites also could produce differences in reactivity relative to TM electrocatalysts. For example, calculations indicate that the P atoms in MoP can stabilize adsorbate species by shifting between hybridization states.[14] Thermodynamic calculations on TM-doped molybdenum sulfide (TM-MoS_2) materials have indicated that CO prefers to adsorb on TM sites, whereas CHO prefers to adsorb on the sulfur sites.[15-16] Consequently, the *CO and *CHO scaling relation might be circumvented on these materials because the intermediates adsorb on fundamentally different catalytic sites. These materials could therefore potentially be more active for CO_2R than TM catalysts, which motivates further studies using *ab initio* calculations to determine whether the H-CO transition state is also stabilized in such systems. Notably, high Faradaic efficiencies have been reported for CO production using MoS_2 and related TM dichalcogenide electrocatalysts.[17-19] However, these studies use the ionic liquid $EMIMBF_4$ (1-ethyl-3-methylimidazolium tetrafluoroborate) as an additive, and ionic liquid additives can lower the overpotential needed to

reduce CO_2 to CO.[20-22] Another study on MoP nanoparticles supported on In-doped carbon showed high Faradic efficiencies toward formate production.[23] This study used the ionic liquid $BMIMPF_6$ (1-butyl-3-methylimidazolium hexafluorophosphate) in a mixture of acetonitrile and water as the electrolyte. Deconvoluting the role of the ionic liquid additive from the intrinsic activity of the TM sulfide and phosphide materials requires further fundamental studies in aqueous electrolytes.

Herein, we demonstrate the process of catalyst screening by using both experiment and theory to evaluate a range of TM sulfide and phosphide materials as CO_2R catalysts in aqueous electrolyte solutions. Both thin film and nanoparticle catalyst morphologies investigated herein showed a high Faradaic efficiency for the HER relative to CO_2R; hence these systems form a primary focus for the combined theoretical and experimental investigations described herein. A thermodynamic analysis indicated that the TM phosphides are selective for the HER relative to CO_2R, due to large differences in their limiting potentials (U_L). While Ni-MoS_2 appears to be promising from a thermodynamic perspective for CO_2R, this sulfide does not sufficiently stabilize the *CO to *CHO transition state energy to allow for high CO_2R activity. These results provide insight into the competition between the HER and CO_2R on TM phosphide and TM sulfide surfaces and highlight the importance of understanding both thermodynamics and kinetics to design more active and selective catalysts for CO_2R.

Nine TM phosphide and five TM sulfide materials were tested as CO_2R catalysts. The thin film catalysts were synthesized by deposition of a thin TM layer on a silicon substrate, followed by vapor-assisted conversion to the phosphide or sulfide.[24-25] SnS films were produced by spin coating FTO (fluorine-doped Sn oxide) substrates with a solution of SnS powder in a mixture of ethylenediamine and 1,2-ethanedithiol.[26-27] TM phosphide nanoparticles were synthesized from tri-*n*-octylphosphine (TOP) and metallic nanoparticles.[28-30] Characterization of these materials can

be found in the Supporting Information. The CO_2R activity of these electrocatalysts was evaluated under 1 atm of CO_2 in 0.10 M potassium bicarbonate at pH 6.8.[7] Current densities greater than 0.1 mA cm^{-2} were investigated to understand the intrinsic catalytic activity of these materials in aqueous electrolytes.

Each of the tested catalysts exhibited a high Faradaic efficiency for H_2 evolution relative to CO_2R (**Figure 1**). Although the intermittent release of hydrogen bubbles led to error in the quantification of evolved H_2 and, thus, sometimes resulted in the calculation of Faradaic efficiencies exceeding 100 percent, this error does not affect the robustness of the conclusions regarding selectivity because H_2 was the dominant product formed by these systems in all cases. Several materials produced trace amounts of methane or small quantities of CO. However, the Faradaic efficiency for all CO_2R products was less than 3.5 percent for each tested material (Table 1), with the HER accounting for the majority of the charge passed during the electrolysis.

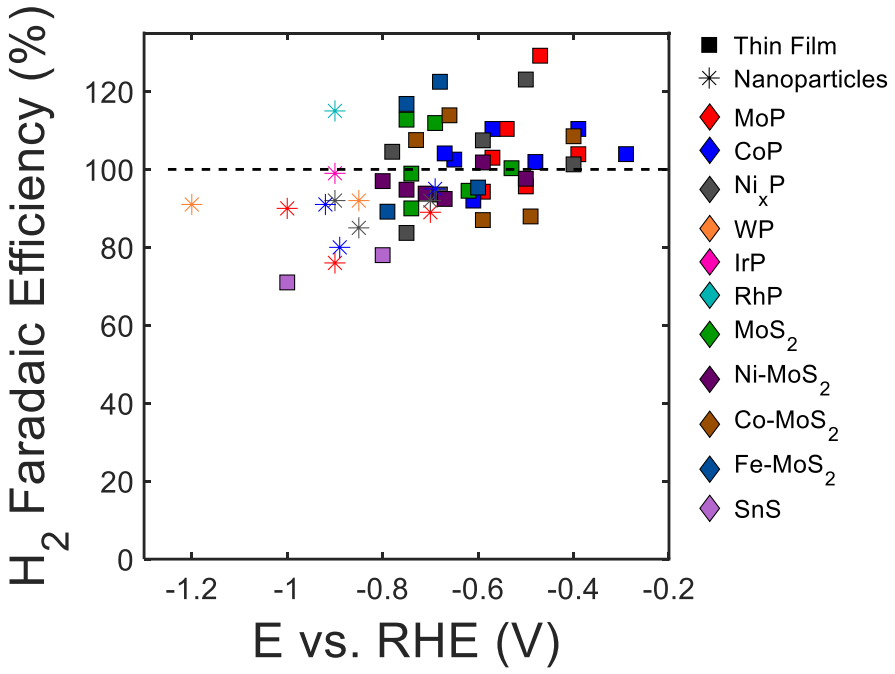

Figure 1. Faradaic efficiency for H_2 production under CO_2R conditions for representative transition metal phosphide and sulfide materials. Less than 3.5 percent of the current

density went towards CO_2 reduction products on these materials. Square symbols denote thin film catalysts while asterisk symbols denote nanoparticle catalysts. The color of the symbol corresponds to the material composition.

Table 1. Summary of Product Distributions for All Tested Materials at a Fixed Potential

material	morphology	potential (V vs. RHE)	current density (mA cm^{-2})	H_2 FE[1] (%)	CO FE[1] (%)	CH_4 FE[1] (%)	$HCOO^-$ FE[1] (%)
MoP	Thin film	-0.54	-5.1(±2.8)	110	0	0	0
CoP	Thin film	-0.65	-4.0(±2.6)	103	0	0	0
Ni_xP	Thin film	-0.75	-3.6 (±2.1)	84	Trace	0	0
MoS_2	Thin film	-0.69	-4.7(±1.5)	112	0	0	0
Ni-MoS_x	Thin film	-0.67	-3.4(±0.9)	92	0	0	0
Co-MoS_x	Thin film	-0.66	-4.0 (±0.2)	114	0	0	0
Fe-MoS_x	Thin film	-0.75	-4.9 (±0.4)	117	0	0	0
SnS	Thin film	-1.00	-1.3 (±0.3)	71	3.4	0	0
MoP	Nanoparticles	-0.90	-4.0 (±0.5)	76	Trace	Trace	Trace
Ni_2P	Nanoparticles	-0.70	-9.7 (±1.5)	92	0	0	0
CoP	Nanoparticles	-0.69	-12.0 (±2.0)	95	0	Trace	0
WP	Nanoparticles	-0.85	-6.2 (±0.8)	92	Trace	Trace	0
IrP	Nanoparticles	-0.90	-11.9 (±2.2)	99	0	0	0
RhP	Nanoparticles	-0.90	-11.4 (±2.5)	115	0	Trace	0

1. FE refers to Faradaic efficiency.

While the phosphides and sulfides showed high selectivity for H_2 production, these catalysts also exhibited a substantial increase in the overpotential needed to drive the HER under CO_2R testing conditions relative to the overpotential measured under traditional HER conditions, such as H_2 purged, 0.50 M H_2SO_4 (**Figure 2**).[24-25] On Au (111), Pt (111), and polycrystalline Ir rotating disk electrodes in 0.10 M $HClO_4$ and $KClO_4$ electrolytes, an additional 350 to 750 mV of overpotential on an RHE scale was required to reach a current density of 10 mA cm^{-2} in a pH 7

electrolyte compared to a pH 1 electrolyte.[31] This shift in HER activity was attributed to a difference in proton donating species, with hydronium acting as the proton donor in acidic pH and water donating protons in neutral pH.[31] However, in a neutral phosphate electrolyte, CoP and FeP electrocatalysts needed only an additional 40 to 50 mV on an RHE scale to produce a cathodic current density of 10 mA cm^{-2}, relative to the overpotentials for the HER in 0.50 M H_2SO_4.[29,32] This result highlights the role of buffering species as potential proton donors, and phosphate species likely contribute to the HER activity in these studies.[33] Under the near-neutral pH CO_2R conditions shown in **Figure 2**, both bicarbonate and water could act as potential sources of protons for the HER.[34] Much remains to be learned regarding the mechanism of proton transfer from buffering anions such as bicarbonate and phosphate to the catalyst surface during the HER, and it is noted that mass transfer could limit the activity at potentials where water cannot be reduced. Further CV experiments using a rotating disk electrode could help elucidate the role of the mass transport of buffer species on HER activity as well as simplify the comparison between the LSV data collected in H_2SO_4 and the steady state chronoamperometric measurements in $KHCO_3$ presented in **Figure 2**. Nevertheless, in addition to pH effects, additional phenomena could be impacting the activity of catalysts under CO_2R conditions.

Previous reports suggest that adsorbed CO can significantly affect the HER activity of metals, since adsorbed CO not only blocks H adsorption sites but also weakens the H binding energy of the surface.[35-37] On metals with CO binding energies stronger than -1 eV, the equilibrium coverage of CO weakens the ΔG of hydrogen adsorption (ΔG_H) by ~ 0.5 eV.[36] Preliminary calculations on CoP (see Supporting Information) suggest that several of the tested materials should have substantial CO coverage at potentials where CO_2R ought to occur. This high CO coverage could weaken the ΔG_H and alter the HER activity on these materials.

To examine this possibility, we tested CoP and MoS_2 thin film electrodes in an Ar, saturated 0.10 M $KHCO_3$ electrolyte. Because this electrolyte is a higher pH (~9.0) than the CO_2 saturated electrolyte (~6.8), we plot the data on both an RHE (**Figure 2a)** and an SHE (**Figure 2b)** potential scale. Calculations (see below) suggest CO binds strongly to CoP while MoS_2 binds CO more weakly. Thus, we would expect the effect of CO adsorption to be greater on CoP than on MoS_2. Indeed, at potentials negative of -0.8 V vs. SHE, the HER activity of CoP appears higher in Ar saturated electrolyte than in CO_2 saturated electrolyte. Additionally, the HER activity for CoP in CO_2 saturated electrolyte shows a significantly different slope than in Ar saturated 0.10 M $KHCO_3$. While ascribing this change in slope to specific mechanistic changes requires further experiment and theory, adsorbed CO has been reported to increase the Tafel slope for the HER on Pt catalysts.[38] This effect will be investigated further in a future work. On MoS_2, however, the HER activity is comparable between CO_2 saturated $KHCO_3$ and Ar saturated electrolyte on an SHE scale. These results suggest that the HER activity on strong CO binding catalysts, such as CoP, is being altered by adsorbed CO; this effect is not observed on weaker CO binding catalysts such as MoS_2.While, the suppression of the HER activity under CO_2R conditions is promising, the low selectivity towards CO_2R suggests that much remains to be learned regarding the competition between these reactions.

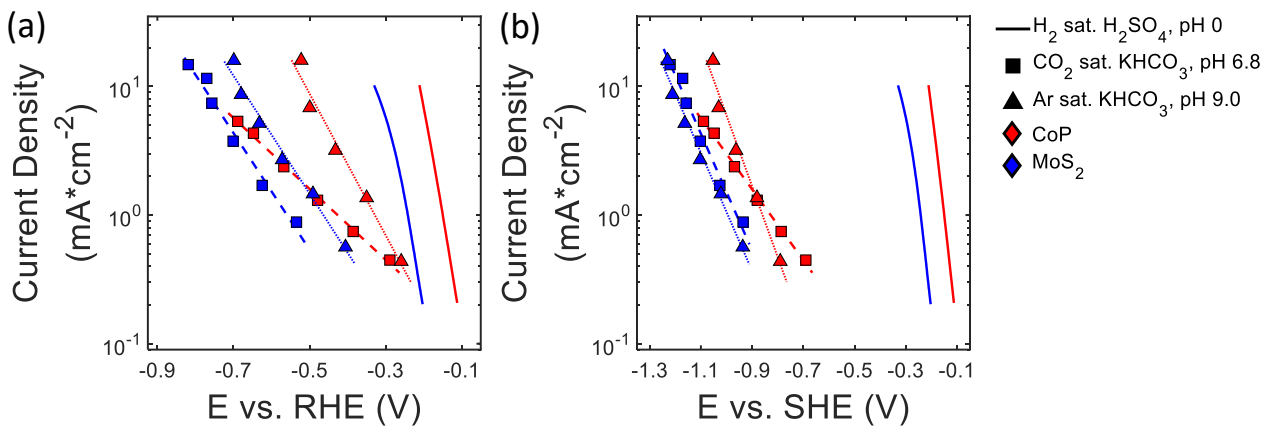

Figure 2. Current density of CoP and MoS_2 thin films under different electrochemical conditions. Sister samples are shown for the Ar and CO_2 saturated electrolytes. Figure 2a is plotted on an RHE potential scale while Figure 2b is plotted on an SHE potential scale. Linear sweep voltammograms in H_2 saturated 0.50 M H_2SO_4 are shown as solid lines. Steady state measurements in CO_2 saturated 0.10 M $KHCO_3$ are denoted as squares and with a dashed line to guide the eye while steady state measurements in Ar saturated 0.10 M $KHCO_3$ are denoted as triangles with a dotted line to guide the eye. Red lines and symbols correspond to measurements using CoP as an electrocatalyst while blue lines and symbols represent measurements using MoS_2.

To understand these experimental results, *ab initio* simulations were performed to gain insight into the selectivity of these materials towards the HER. Determination of electrochemical transition states requires explicit consideration of potential, ions, and solvating water molecules, all of which present open challenges.[39-40] Consequently, we describe herein an iterative computational screening process, beginning with an idealized thermodynamic analysis of the CO to CHO and HER steps[9] and subsequently pursuing computationally intensive determinations of the associated activation barriers for the most promising electrocatalyst candidates.

In previous studies on TM catalysts, thermodynamic calculations of the *CO to *CHO step provided a useful first description of the theoretical overpotential needed to reduce CO_2 past *CO.[9] On Cu, for example, *CO and *CHO have comparable and moderate binding energies, leading to moderate overpotentials for CO_2R to hydrocarbons and oxygenates. For TM phosphide and sulfide surfaces, *CO and *CHO preferentially bind to metal and phosphorus/sulfur sites, respectively. This behavior may in part be attributed to the bifunctional nature of these surfaces. The lone pair of CO acts as a Lewis base and back-bonds with metals upon adsorption.[13,41] Therefore, if both metal and phosphorous/sulfur sites are exposed on a facet, the *CO intermediate tends to preferentially bind to the metal (Supporting Information).

Figure 3a presents the bifunctional stabilization of these intermediates by plotting the binding energy of CHO vs. CO. This benchmark serves as a simple means to compare the behavior of different electrocatalysts. The *CHO intermediate is stabilized when bound to undercoordinated S-edge sites. On MoS_2 and doped MoS_2, this stabilization at edges pushes these catalysts into a region of thermodynamic interest, where *CO is bound moderately and comparably to *CHO. Unlike these sulfides, most phosphides fall near the (211) and (111) TM scaling lines. For these surfaces, even though *CHO preferentially binds to P-sites, the stabilization of P-*CHO relative to M-*CHO is marginal. Based on thermodynamic criteria alone and assuming that the activation energies scale with the difference between the initial and final state energies, phosphides are therefore unlikely to yield reduced overpotentials for CO_2R.[42]

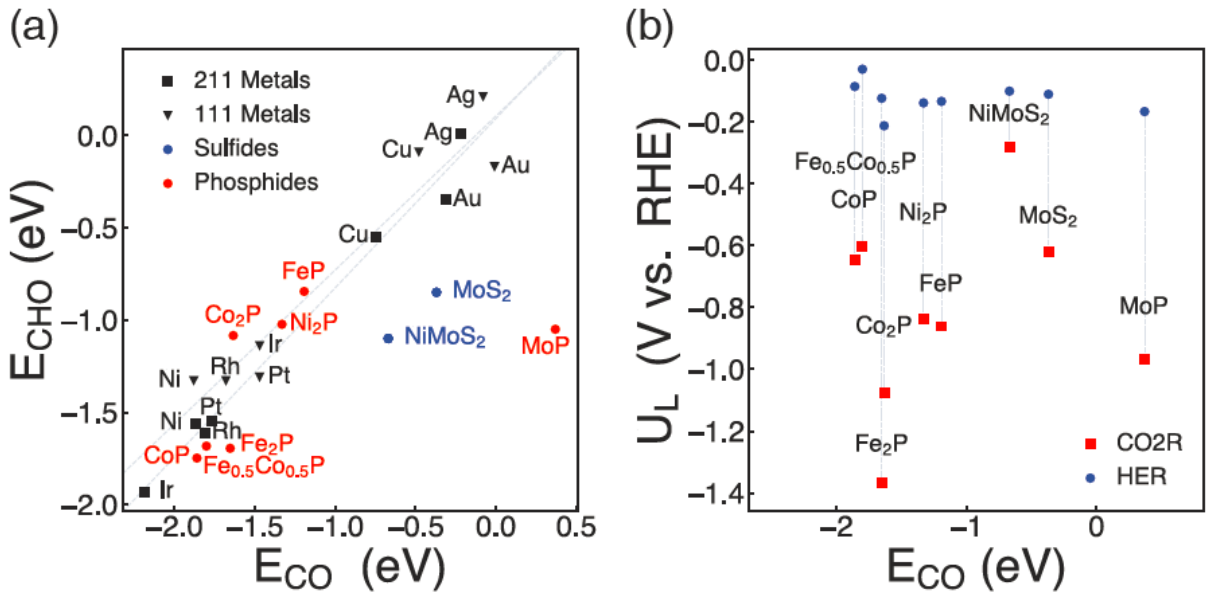

Figure 3. a. Traditional thermodynamic screening criteria for CO_2R, showing the binding energy of CHO versus CO on surfaces at equilibrium hydrogen coverage. b. Corresponding theoretical U_L for HER and CO_2R, calculated as the free energy difference of the *CO to *CHO step for strong binding surfaces, and the free energy difference of the *COOH to *CO step for weak binding surfaces (MoP).

One deviation from thermodynamic scaling in **Figure 3a** requires further discussion. The (001) MoP surface is P-terminated, and geometric constraints prevent any direct binding between adsorbates and metal sites. The P-sites interact with *CO weakly and *CHO strongly, differentiating between the two adsorbates and leading to the apparent deviation from the thermodynamic scaling line. This weakened interaction has been ascribed to shifts in hybridization of the P-site as well as possible lone pair repulsion of CO.[14] However, CO binding is very weak on MoP, and hence desorption is favored relative to further reduction of *CO.

Thermodynamic screening criteria for CO_2R indicate that TM sulfides are promising electrocatalyst candidates, but the CO_2R pathway must be compared to the competing HER. Hence, theoretical U_L values were calculated for the HER and CO_2R (**Figure 3b**). The U_L is a

theoretical estimation of the minimum voltage which must be applied for a reaction step to become downhill in free energy and is defined as the min(-ΔG(U=0)/e) of all elementary steps along a reduction path.[36] For TM surfaces, on which the activation and reaction energies scale, this measure has been a useful descriptor of activity,[43-46] with trends in selectivity also shown to follow the difference in HER and CO_2R U_L.[15,36] Previously, a value of $|U_{L\ CO2R} - U_{L\ HER}| < 0.5$ V was experimentally associated with metals for which the HER activity does not dominate relative to CO_2R.[15] For all the phosphides considered, the difference in U_L is 0.6 V or greater, suggesting that a high selectivity for CO_2R is unlikely without substantial suppression of the HER, a major challenge.[47] This expectation is supported by the experimentally measured Faradaic efficiencies, which show a high selectivity for H_2 production relative to CO_2R. However, this limiting potential criterion suggests that Ni-MoS_2 holds potential for high activity and selectivity for CO_2R.

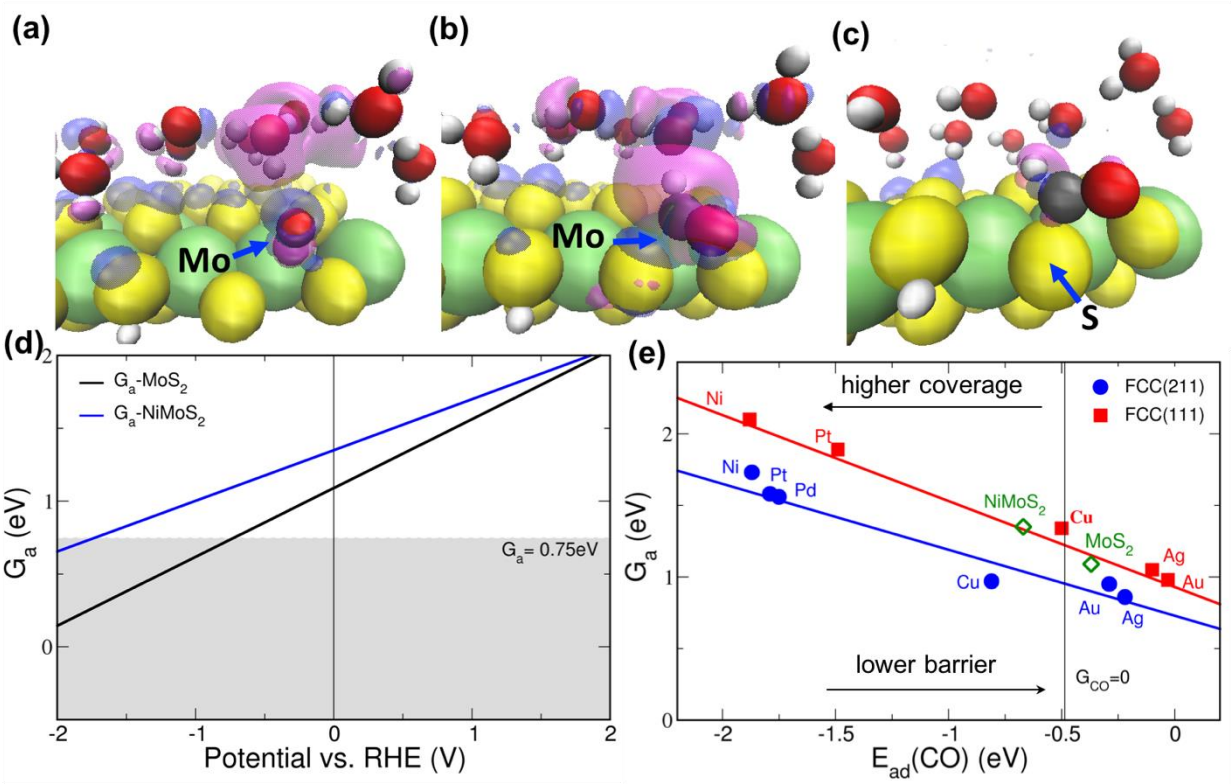

Figure 4. The charge density differences for *CO (Figure 4a), H-CO (Figure 4b), and *CHO (Figure 4c) on MoS_2. The blue and magenta isosurfaces correspond to charge densities of –0.001 e Bohr^{-3} and 0.001 e Bohr^{-3}, respectively. d. Potential-dependent barriers for CO→CHO on MoS_2 and Ni-MoS_2 at 0V vs RHE and pH 7, with respect to a threshold value of 0.75 eV. e. The barrier for CO→CHO on MoS_2 and Ni-MoS_2 compared to face-centered cubic transition metal (111) and (211) facets.

Having passed this "first round" of thermodynamics-based screening criteria, Ni-MoS_2 was further investigated for its corresponding electrochemical activation energies. MoS_2 was also examined as a point of comparison. **Figure 4a-c** shows the charge density isosurfaces for the *CO→*CHO barrier on MoS_2 and illustrates the shift in charge density within the cell during the proton-electron transfer. The constant potential activation free energies were determined from these constant-charge calculations, using a charge-extrapolation scheme based on a capacitor model of the interface.[39,48] The resulting barriers are shown as a function of potential in **Figure 4d**.

The incorporation of kinetic criteria leads to an improved estimation of the catalytic activity relative to that obtained by thermodynamic predictions alone. The kinetic barriers at 0 V vs. RHE for CO protonation at the MoS_2 and Ni-MoS_2 edge sites were calculated to be 1.09 eV and 1.35 eV, respectively. As indicated in **Figure 4d**, a barrier of 0.75 eV, equivalent to a turnover frequency of one per site per second at room temperature, was defined as the threshold for facile kinetics. Given a transfer coefficient of 0.47 for MoS_2 and 0.35 for Ni-MoS_2 (See SI for β calculation details), overcoming the kinetic barriers to produce CO_2R products becomes facile at potentials of -0.72 V and -1.71 V vs. RHE, respectively.

MoS_2 was calculated to possess a surmountable kinetic barrier for CO protonation, but the calculated ΔG_{CO} is weak (0.1 eV), which should limit formation of further reduced products.[10] Furthermore, the $|U_{L\ CO2R} - U_{L\ HER}|$ for MoS_2 lies above the 0.5 V threshold above which on transition metals the HER dominates over CO_2R. For Ni-MoS_2, the ΔG_{CO} is calculated to be -0.20 eV, similar to that of Cu (211); sufficiently negative free energies favor *CO coverage over desorption, allowing for further reduction. However, the activation barrier remains prohibitively high. The physical rationale behind this high barrier lies in the transition state geometry. At the transition and final states, the S-C distance is calculated to be 2.2 Å and 1.8 Å, respectively, which suggests a loosely bound transition state. Therefore, the stabilization imparted from S-sites on *CHO binding does not necessarily stabilize the transition state energy.

Calculations indicate that CO rotates to expose the carbon during proton-electron transfer, and the activation energy would therefore decrease with weaker *CO binding (**Figure 4e)**.[10] Neither MoS_2 nor Ni-MoS_2 exhibit a substantial deviation from the activation energy scaling lines characteristic of TM electrocatalysts, illustrating that the activation energy is determined by *CO binding rather than *CHO binding. Achieving lower kinetic barriers for CO protonation will thus require exploration of a narrower window of CO binding energies, between Ni-MoS_2 and MoS_2, or unique sites with more rotational degrees of freedom. The calculations indicate that the considered TM phosphides and sulfides do not meet these criteria, in accord with the experimentally observed Faradaic efficiencies favoring the HER relative to CO_2R. These observations emphasize the importance of considering activation energies in the search for new CO_2R catalysts, and indicate that surmountable thermodynamic pathways alone, while necessary, are not a sufficient criterion for high activity.

Having explored a range of metal phosphide and sulfide catalysts, all were found to be more selective for the HER than for CO_2R. We provide one possible explanation for this low CO_2R selectivity using computational insights. Calculations indicate that strong binding transition metal phosphides, like their transition metal counterparts, show a substantially smaller U_L for the HER than for CO_2R. Microkinetic modeling of the full path should be undertaken to draw concrete conclusions about whether this phenomenological criterion holds for transition metal phosphides and sulfides, as well. Binding energy and U_L calculations suggest that Ni-MoS_2 could be a promising CO_2R catalyst; however, the calculated kinetic barrier for the proton-electron transfer to *CO is too high to allow for facile kinetics. The combination of experiment and theory provides a more complete understanding of the competition between the HER and CO_2R for these systems and motivates the exploration of methods to suppress the HER during CO_2R.[47]

Experimental Methods

Molybdenum sulfide and TM phosphide thin films were synthesized as described previously.[24-25] A thin film of the TM was deposited onto a silicon substrate using electron beam physical vapor deposition. The metal thin films were then converted to the phosphide or sulfide through a vapor-assisted process in a tube furnace. Thin films of SnS were produced by spin coating a solution of SnS powder onto FTO.[26-27] The nanoparticle catalysts were synthesized by heating metallic nanoparticles in a mixture of of tri-*n*-octyphosphine, 1-octadecene, and oleylamine was heated for 1 h under vacuum (*Caution:* All nanoparticle synthesis was performed in a fume hood to limit exposure to reagents such as trioctylphosphine and oleylamine, which can cause chemical burns).[28,30,49] The materials were evaluated for CO_2R activity in a flow cell that contained CO_2-sparged 0.10 M $KHCO_3$.[7] The experimental methodology is described in more detail in the Supporting Information.

The lattice constants and optimization parameters for DFT calculations have been described previously,[10,16,50] with further calculation details provided in the Supporting Information. A Bravais-Friedel-Donnay-Harker crystal morphology algorithm identified the most probable facets based on geometric considerations.[51-52] On each of these low index surface terminations, free energy adsorption analysis was used to identify the most active facet, providing an estimate for the peak activity that may be observed experimentally. All reported free energies ($G = E + E_{ZPE} - TS$) are estimated by including zero point energies and entropy contributions calculated in the harmonic approximation. The free energy and electronic binding energies of adsorption for all intermediates are referenced to their gas phase counterparts. For example, $\Delta G_{CO} = G_{*CO} - (G_{slab} + G_{CO\,(g)})$.

Supporting Information

Expanded details on synthesis, experimental methods, and computational methods; X-ray photoelectron spectroscopy of synthesized phosphides and sulfides; calculation of CO coverage on CoP; CO binding and charge density differences; complete product distribution for catalysts studied; and the tabulated values used to prepare figures.

Acknowledgements

This material is based, in part, on work performed by the Joint Center for Artificial Photosynthesis, a DOE Energy Innovation Hub, supported through the Office of Science of the U.S. Department of Energy, under Award No. DE-SC0004993. This research used resources of the National Energy Research Scientific Computing Center, a DOE Office of Science User Facility supported by the Office of Science of the U.S. Department of Energy (under Contract No. DE-AC02-05CH11231). Part of this work was performed at the Stanford Nano Shared Facilities (SNSF) and the Stanford Nanofabrication Facility (SNF), supported by the National Science Foundation under Award ECCS-1542152. We also acknowledge assistance from the Stanford NMR Facility. M.F. and D.A.T. acknowledge a graduate fellowship through the National Science Foundation. S.A.F. acknowledges the Resnick Sustainability Institute at Caltech for a postdoctoral fellowship. The authors would also like to thank J. Chance Crompton for assistance in synthesizing the nanoparticle electrocatalysts.

References

(1). Whipple, D.; Kenis, P. Prospects of CO_2 Utilization via Direct Heterogeneous Electrochemical Reduction. *J. Phys. Chem. Lett.* **2010,** *1*, 3451-3458.

(2). Kortlever, R.; Shen, J.; Schouten, K.; Calle-Vallejo, F.; Koper, M. Catalysts and Reaction Pathways for the Electrochemical Reduction of Carbon Dioxide. *J. Phys. Chem. Lett.* **2015,** *6*, 4073-4082.

(3). Jovanov, Z.; Hansen, H.; Varela, A.; Malacrida, P.; Peterson, A.; Nørskov, J.; Stephens, I.; Chorkendorff, I. Opportunities and Challenges in the Electrocatalysis of CO_2 and CO Reduction Using Bifunctional Surfaces: A Theoretical and Experimental Study of Au-Cd Alloys. *J. Catal.* **2016,** *343*, 215-231.

(4). Hori, Y. Electrochemical CO_2 Reduction on Metal Electrodes. In *Modern Aspects of Electrochemistry, No 42*, Vayenas, C. G.; White, R. E.; Gamboa-Aldeco, M. E., Eds. 2008; pp 89-189.

(5). Qiao, J.; Liu, Y.; Hong, F.; Zhang, J. A Review of Catalysts for the Electroreduction of Carbon Dioxide to Produce Low-Carbon Fuels. *Chem. Soc. Rev.* **2014,** *43*, 631-675.

(6). Lewis, N.; Nocera, D. Powering the Planet: Chemical Challenges in Solar Energy Utilization. *Proc. Natl. Acad. Sci. U. S. A.* **2007,** *104*, 20142-20142.

(7). Kuhl, K.; Cave, E.; Abram, D.; Jaramillo, T. New Insights into the Electrochemical Reduction of Carbon Dioxide on Metallic Copper Surfaces. *Energy Environ. Sci.* **2012,** *5*, 7050-7059.

(8). Singh, M.; Clark, E.; Bell, A. Effects of Electrolyte, Catalyst, and Membrane Composition and Operating Conditions on the Performance of Solar-Driven Electrochemical Reduction of Carbon Dioxide. *Phys. Chem. Chem. Phys.* **2015,** *17*, 18924-18936.

(9). Peterson, A.; Nørskov, J. Activity Descriptors for CO_2 Electroreduction to Methane on Transition-Metal Catalysts. *J. Phys. Chem. Lett.* **2012,** *3*, 251-258.

(10). Liu, X.; Xiao, J.; Peng, H.; Hong, X.; Chan, K.; Nørskov, J. K. Understanding Trends in Electrochemical Carbon Dioxide Reduction Rates. *Nat. Commun.* **2017,** *8*, 15438.

(11). Abild-Pedersen, F. Computational Catalyst Screening: Scaling, Bond-Order and Catalysis. *Catal. Today* **2016,** *272*, 6-13.

(12). Montoya, J. H.; Seitz, L. C.; Chakthranont, P.; Vojvodic, A.; Jaramillo, T. F.; Nørskov, J. K. Materials for Solar Fuels and Chemicals. *Nat. Mater.* **2017,** *16*, 70-81.

(13). Lee, Y.; Oyama, S. Bifunctional Nature of a SiO_2-Supported Ni_2P Catalyst for Hydrotreating: EXAFS and FTIR Studies. *J. Catal.* **2006,** *239*, 376-389.

(14). Fields, M.; Tsai, C.; Chen, L.; Abild-Pedersen, F.; Nørskov, J.; Chan, K. Scaling Relations for Adsorption Energies on Doped Molybdenum Phosphide Surfaces. *ACS Catal.* **2017,** *7*, 2528-2534.

(15). Chan, K.; Tsai, C.; Hansen, H. A.; Nørskov, J. K. Molybdenum Sulfides and Selenides as Possible Electrocatalysts for CO_2 Reduction. *ChemCatChem* **2014,** *6*, 1899-1905.

(16). Hong, X.; Chan, K.; Tsai, C.; Nørskov, J. How Doped MoS_2 Breaks Transition-Metal Scaling Relations for CO_2 Electrochemical Reduction. *ACS Catal.* **2016,** *6*, 4428-4437.

(17). Asadi, M.; Kumar, B.; Behranginia, A.; Rosen, B. A.; Baskin, A.; Repnin, N.; Pisasale, D.; Phillips, P.; Zhu, W.; Haasch, R., et al. Robust Carbon Dioxide Reduction on Molybdenum Disulphide Edges. *Nat. Commun.* **2014,** *5*, 4470.

(18). Asadi, M.; Kim, K.; Liu, C.; Addepalli, A.; Abbasi, P.; Yasaei, P.; Phillips, P.; Behranginia, A.; Cerrato, J.; Haasch, R., et al. Nanostructured Transition Metal Dichalcogenide Electrocatalysts for CO_2 Reduction in Ionic Liquid. *Science* **2016,** *353*, 467-470.

(19). Abbasi, P.; Asadi, M.; Liu, C.; Sharifi-Asl, S.; Sayahpour, B.; Behranginia, A.; Zapol, P.; Shahbazian-Yassar, R.; Curtiss, L.; Salehi-Khojin, A. Tailoring the Edge Structure of Molybdenum Disulfide toward Electrocatalytic Reduction of Carbon Dioxide. *ACS Nano* **2017,** *11*, 453-460.
(20). Rosen, B.; Salehi-Khojin, A.; Thorson, M.; Zhu, W.; Whipple, D.; Kenis, P.; Masel, R. Ionic Liquid-Mediated Selective Conversion of CO_2 to CO at Low Overpotentials. *Science* **2011,** *334*, 643-644.
(21). Rosen, B.; Haan, J.; Mukherjee, P.; Braunschweig, B.; Zhu, W.; Salehi-Khojin, A.; Dlott, D.; Masel, R. In Situ Spectroscopic Examination of a Low Overpotential Pathway for Carbon Dioxide Conversion to Carbon Monoxide. *J. Phys. Chem. C* **2012,** *116*, 15307-15312.
(22). Wang, Y.; Hatakeyama, M.; Ogata, K.; Wakabayashi, M.; Jin, F.; Nakamura, S. Activation of CO_2 by Ionic Liquid EMIM-BF4 in the Electrochemical System: A Theoretical Study. *Phys. Chem. Chem. Phys.* **2015,** *17*, 23521-23531.
(23). Sun, X.; Lu, L.; Zhu, Q.; Wu, C.; Yang, D.; Chen, C.; Han, B. MoP Nanoparticles Supported on Indium-Doped Porous Carbon: Outstanding Catalysts for Highly Efficient CO_2 Electroreduction. *Angew. Chem. Int. Ed.* **2018,** *57*, 2427-2431.
(24). Benck, J. D.; Lee, S. C.; Fong, K. D.; Kibsgaard, J.; Sinclair, R.; Jaramillo, T. F. Designing Active and Stable Silicon Photocathodes for Solar Hydrogen Production Using Molybdenum Sulfide Nanomaterials. *Adv. Energy Mater.* **2014,** *4*, 1400739.
(25). Hellstern, T. R.; Benck, J. D.; Kibsgaard, J.; Hahn, C.; Jaramillo, T. F. Engineering Cobalt Phosphide (CoP) Thin Film Catalysts for Enhanced Hydrogen Evolution Activity on Silicon Photocathodes. *Adv. Energy Mater.* **2016,** *6*, 1501758.
(26). Antunez, P. D.; Torelli, D. A.; Yang, F.; Rabuffetti, F. A.; Lewis, N. S.; Brutchey, R. L. Low Temperature Solution-Phase Deposition of SnS Thin Films. *Chem. Mater.* **2014,** *26*, 5444-5446.
(27). Webber, D. H.; Brutchey, R. L. Alkahest for V_2VI_3 Chalcogenides: Dissolution of Nine Bulk Semiconductors in a Diamine-Dithiol Solvent Mixture. *J. Am. Chem. Soc.* **2013,** *135*, 15722-15725.
(28). Henkes, A.; Schaak, R. Trioctylphosphine: A General Phosphorus Source for the Low-Temperature Conversion of Metals into Metal Phosphides. *Chem. Mater.* **2007,** *19*, 4234-4242.
(29). Callejas, J.; McEnaney, J.; Read, C.; Crompton, J.; Biacchi, A.; Popczun, E.; Gordon, T.; Lewis, N.; Schaak, R. Electrocatalytic and Photocatalytic Hydrogen Production from Acidic and Neutral-pH Aqueous Solutions Using Iron Phosphide Nanoparticles. *ACS Nano* **2014,** *8*, 11101-11107.
(30). Callejas, J.; Read, C.; Roske, C.; Lewis, N.; Schaak, R. Synthesis, Characterization, and Properties of Metal Phosphide Catalysts for the Hydrogen-Evolution Reaction. *Chem. Mater.* **2016,** *28*, 6017-6044.
(31). Strmcnik, D.; Uchimura, M.; Wang, C.; Subbaraman, R.; Danilovic, N.; van der Vliet, D.; Paulikas, A. P.; Stamenkovic, V. R.; Markovic, N. M. Improving the Hydrogen Oxidation Reaction Rate by Promotion of Hydroxyl Absorption. *Nat. Chem.* **2013,** *5*, 300-306.
(32). Tian, J.; Liu, Q.; Asiri, A.; Sun, X. Self-Supported Nanoporous Cobalt Phosphide Nanowire Arrays: An Efficient 3D Hydrogen-Evolving Cathode over the Wide Range of pH 0-14. *J. Am. Chem. Soc.* **2014,** *136*, 7587-7590.
(33). Ooka, H.; Figueiredo, M. C.; Koper, M. T. M. Competition between Hydrogen Evolution and Carbon Dioxide Reduction on Copper Electrodes in Mildly Acidic Media. *Langmuir* **2017,** *33*, 9307-9313.

(34). Resasco, J.; Lum, Y.; Clark, E.; Zeledon, J. Z.; Bell, A. T. Effects of Anion Identity and Concentration on Electrochemical Reduction of CO_2. *ChemElectroChem* **2018,** *5*, Early View.
(35). Zhang, Y.-J.; Sethuraman, V.; Michalsky, R.; Peterson, A. A. Competition between CO_2 Reduction and H_2 Evolution on Transition-Metal Electrocatalysts. *ACS Catal.* **2014,** *4*, 3742-3748.
(36). Shi, C.; Hansen, H.; Lausche, A.; Nørskov, J. Trends in Electrochemical CO_2 Reduction Activity for Open and Close-Packed Metal Surfaces. *Phys. Chem. Chem. Phys.* **2014,** *16*, 4720-4727.
(37). Cave, E. R.; Shi, C.; Kuhl, K. P.; Hatsukade, T.; Abram, D. N.; Hahn, C.; Chan, K.; Jaramillo, T. F. Trends in the Catalytic Activity of Hydrogen Evolution during CO_2 Electroreduction on Transition Metals. *ACS Catal.* **2018,** *8*, 3035-3040.
(38). Kita, H.; Ye, S.; Sugimora, K. Effects of Adsorbed CO on the Electrode Reactions at a Platinum Electrode. *J. Electroanal. Chem.* **1991,** *297*, 283-296.
(39). Chan, K.; Nørskov, J. K. Electrochemical Barriers Made Simple. *J. Phys. Chem. Lett.* **2015,** *6*, 2663-2668.
(40). Schnur, S.; Gross, A. Challenges in the First-Principles Description of Reactions in Electrocatalysis. *Catal. Today* **2011,** *165*, 129-137.
(41). Infantes-Molina, A.; Gralberg, E.; Cecilia, J.; Finocchio, E.; Rodriguez-Castellon, E. Nickel and Cobalt Phosphides as Effective Catalysts for Oxygen Removal of Dibenzofuran: Role of Contact Time, Hydrogen Pressure and Hydrogen/Feed Molar Ratio. *Catal. Sci. Technol.* **2015,** *5*, 3403-3415.
(42). Wang, S.; Petzold, V.; Tripkovic, V.; Kleis, J.; Howalt, J.; Skulason, E.; Fernandez, E.; Hvolbaek, B.; Jones, G.; Toftelund, A., et al. Universal Transition State Scaling Relations for (De)Hydrogenation Over Transition Metals. *Phys. Chem. Chem. Phys.* **2011,** *13*, 20760-20765.
(43). Peterson, A.; Abild-Pedersen, F.; Studt, F.; Rossmeisl, J.; Nørskov, J. How Copper Catalyzes the Electroreduction of Carbon Dioxide into Hydrocarbon Fuels. *Energy Environ. Sci.* **2010,** *3*, 1311-1315.
(44). Man, I.; Su, H.; Calle-Vallejo, F.; Hansen, H.; Martinez, J.; Inoglu, N.; Kitchin, J.; Jaramillo, T.; Nørskov, J.; Rossmeisl, J. Universality in Oxygen Evolution Electrocatalysis on Oxide Surfaces. *ChemCatChem* **2011,** *3*, 1159-1165.
(45). Greeley, J.; Stephens, I.; Bondarenko, A.; Johansson, T.; Hansen, H.; Jaramillo, T.; Rossmeisl, J.; Chorkendorff, I.; Nørskov, J. Alloys of Platinum and Early Transition Metals as Oxygen Reduction Electrocatalysts. *Nat. Chem.* **2009,** *1*, 552-556.
(46). Nørskov, J.; Bligaard, T.; Logadottir, A.; Kitchin, J.; Chen, J.; Pandelov, S. Trends in the Exchange Current for Hydrogen Evolution. *J. Electrochem. Soc.* **2005,** *152*, J23-J26.
(47). Singh, A.; Rohr, B.; Schwalbe, J.; Cargnello, M.; Chan, K.; Jaramillo, T.; Chorkendorff, I.; Nørskov, J. Electrochemical Ammonia Synthesis-The Selectivity Challenge. *ACS Catal.* **2017,** *7*, 706-709.
(48). Chan, K.; Nørskov, J. K. Potential Dependence of Electrochemical Barriers from ab Initio Calculations. *J. Phys. Chem. Lett.* **2016,** *7*, 1686-1690.
(49). Popczun, E.; McKone, J.; Read, C.; Biacchi, A.; Wiltrout, A.; Lewis, N.; Schaak, R. Nanostructured Nickel Phosphide as an Electrocatalyst for the Hydrogen Evolution Reaction. *J. Am. Chem. Soc.* **2013,** *135*, 9267-9270.
(50). Kibsgaard, J.; Tsai, C.; Chan, K.; Benck, J.; Nørskov, J.; Abild-Pedersen, F.; Jaramillo, T. Designing an Improved Transition Metal Phosphide Catalyst for Hydrogen Evolution Using Experimental and Theoretical Trends. *Energy Environ. Sci.* **2015,** *8*, 3022-3029.

(51). Bajdich, M.; Garcia-Mota, M.; Vojvodic, A.; Nørskov, J.; Bell, A. Theoretical Investigation of the Activity of Cobalt Oxides for the Electrochemical Oxidation of Water. *J. Am. Chem. Soc.* **2013,** *135*, 13521-13530.
(52). Docherty, R.; Clydesdale, G.; Roberts, K.; Bennema, P. Application of Bravais-Friedel-Donnay-Harker, Attachment Energy and Ising Models to Predicting and Understanding the Morphology of Molecular Crystals. *J. Phys. D: Appl. Phys.* **1991,** *24*, 89-99.